AIAA 82-4162

Flow Control for an Airborne Laser Turret

James R. Schonberger,* Allen E. Fuhs,† and Alan M. Mandigo‡
Naval Postgraduate School, Monterey, Calif.

A high-energy laser system inflicts damage on a target by radiating large amounts of thermal energy onto a small area. Airflow about a laser pointer-tracker turret on an aircraft may be unsteady, causing problems in laser beam propagation. These problems are jitter, which is vibration of the laser beam, and optical path distortions. Several airflow control techniques were considered as possible means of suppressing the unsteady flow. A hollow fairing with suction inlets located behind the turret combined with fuselage boundary-layer suction at the turret base was selected as a method of flow control. A 0.3 scale model of the turret and fairing was tested in a wind tunnel at the Naval Postgraduate School. Various turret/fairing geometrical parameters were investigated, as well as flow rates through the suction apparatus. A condition of steady flow around the turret with minimum suction requirements was sought. A turret with 0.427 m diam was tested in the Naval Postgraduate School 1.525 × 1.525-m wind tunnel at a Reynolds number of 300,000. The Reynolds number was defined as VD/ν, where V is tunnel velocity, D is turret diameter, and ν is kinematic viscosity, all quantities being measured in consistent units. Steady flow was achieved with a flow factor F equal to 0.4. F is the ratio A_∞/A_t, where A_∞ is area of streamtube at freestream conditions entering the suction inlets, and A_t is the projected area of laser turret.

Introduction

A HIGH-ENERGY laser weapon system inflicts damage on a target by radiating large amounts of thermal energy onto a small area. The main components of the system are the laser, which generates high-power radiation, and the beam control subsystem, which aims the laser beam at the target. The airborne portion of the Department of Defense (DOD) High Energy Laser (HEL) Program is being developed at the Air Force Weapons Laboratory, Kirtland Air Force Base, N.Mex. The test bed for the program is the Airborne Laser Laboratory (ALL), which consists of two highly instrumented NKC-135 aircraft.

The laser beam is aimed at the target by the pointer tracker, which is part of the beam control subsystem. The pointer tracker is housed on the top of the aircraft inside an optical system turret. In flight, the airflow around the turret causes problems in beam control. The beam control problems are jitter and optical path distortions (OPD). Jitter is a motion of the laser beam that smears the energy focused within a small spot into a larger spot. The dwell time required to damage the target is increased. Jitter is caused, in part, by unsteady pressure loads on the turret and optical components. Optical path distortions, steady and unsteady, are due to shear layers, boundary layers, flow separation, and vortex shedding in the rear of the turret. The flow also causes increased pressure loading on the turret owing to the separated flow region behind the turret. This increased unsteady pressure is caused by turbulence within the recirculation region. The propagation of a laser beam through turbulence can be a major problem.

Research and experimentation have demonstrated that optical distortion caused by unsteady flow cannot be corrected completely by adaptive optical systems, even when utilizing state-of-the-art technology. Information concerning propagation from turrets on aircraft can be found in Otten,[1] Gilbert,[2] Walterick and VanKuren,[3] and McDermott and VanKuren.[4]

The primary objective of this research was to develop a quiescent airflow around the turret so that jitter and optical path distortions were minimized. Control of flow separation will ensure that flow will be quiescent well past the current 120-deg point in order that a greater rearward angle can be achieved by the pointer tracker.

The purpose of this paper is to report the experimental results of the research. An in-depth analysis of these results was not performed.

Viscous Effects and Flow Separation

From potential flow theory, the velocity and static pressure coefficient at the surface of a cylinder or sphere can be calculated. In the direction of flow from the $\theta = 90$-deg position, the static pressure increases toward the rear stagnation point at $\theta = 180$ deg. As discussed by Schlichting,[5] the adverse pressure gradient causes flow separation. The separated flow region consists of shed vortices and a recirculation region bounded by a shear layer. The base flow is intensely turbulent. The turbulent flow adversely affects propagation of laser beams.

Flow separation can be eliminated by at least two methods involving suction. One method, which will be discussed shortly, removes the boundary layer by suction through a porous surface of the turret. A second method eliminates the adverse pressure gradient by suction within the base flow region. Suction can cause either a neutral or a favorable pressure gradient between $\theta = 90$ and 180 deg. The concept of flow control using a favorable pressure gradient is the essence of this research.

Blowing is an alternate method for controlling flow separation. Activation of the boundary layer by blowing nearly tangentially to the surface can delay or prevent separation.

Proposed Flow Control Methods

The following recently proposed methods were presented at a workshop titled Control of Turbulent, Separated Airflow about Aircraft Turrets, sponsored by the Air Force Weapons Laboratory, Kirtland Air Force Base, N.Mex., on March 10 and 11, 1980.[6]

Received Feb. 12, 1981; revision received Nov. 4, 1981. This paper is declared a work of the U.S. Government and therefore is in the public domain.

*Graduate Student. Present address: NAVSEA, Code 62Y13, Washington, D.C.

†Distinguished Professor, Department of Aeronautics. Fellow AIAA.

‡Graduate Student. Present address: USS James K. Polk, SSBN 645 Blue.

1. Porous Standpipe Control

The porous standpipe method uses suction through a perforated cylindrical standpipe located behind the turret. The diameter of the standpipe is one-third the diameter of the turret. The standpipe suction creates a low-pressure area behind the turret, and the airflow remains steady.

2. Slot Blowing

The slot blowing method uses high-velocity air jets blown tangentially along the surface of the turret, activating the boundary layer and preventing separated flow. The internal ducting required for the air jets complicates turret design.

3. Base Suction with Trapped Vortices

The base suction with trapped vortices method uses a fairing located very close to the turret with suction through ports in the fuselage. The fairing has indented grooves immediately downstream of the turret. Suction at the end of the grooves is used to create, stabilize, and remove vorticity shed into the turret wake.

4. Distributed Turret Base Suction

The distributed base suction method utilizes suction through an array of small holes on the rearward side of the turret which effectively removes the boundary layer in this region. The turret design is complicated, however, by the requirement that the turret turns but the suction holes must remain downstream. Additional complexity arises from the necessary ducting within the turret.

5. Fairing Suction

The fairing suction method has suction ports located in the fairing; suction ports are *not* located in the turret. In contrast with the distributed turret base suction, the laser turret is not altered. Flow separation is prevented indirectly with the fairing suction method; the boundary layer on the turret is not directly influenced. The fairing suction method requires larger suction flow rates than the distributed turret base suction; however, the turret is not altered by the fairing suction.

Experimental Apparatus

Overview

A fairing suction method was selected, and apparatus was designed for use in this research project. The hardware consists of the turret, fuselage boundary-layer bleed, hollow fairing, two different fairing nosepieces, and a blower to provide suction.

The fairing suction apparatus uses suction through a hollow fairing nosepiece at the rear of the turret. Figure 1 is a drawing which shows the installation of the test apparatus in the wind-tunnel test section.

In contrast to the laminar flow control methods used on aircraft wings, the turret flow control uses large ducts. Laminar flow control for drag reduction uses thin slots and is susceptible to blockage by insects and dust. The flow control for the laser turret is not sensitive to insects or dust owing to the large size of the suction ports. For perspective of the turret and fairing, see Fig. 2.

A feature of the flow control technique is the fact that modification of the turret is not required although the aircraft modifications may be extensive.

Wind Tunnel

Wind-tunnel tests were conducted in the Naval Postgraduate School 1.525×1.525-m, low-speed tunnel at a maximum velocity of 10 m/s. This tunnel was chosen because of availability and physical size. With the 0.3 scale turret model ($D = 0.427$ m), a Reynolds number of about 3×10^5 was achieved. According to Schlichting,[5] the value of the Reynolds number for the tests is within the critical range, and transition to a turbulent boundary layer will occur on the turret. As tunnel speed was increased slowly from 0 to 10 m/s, the flow separation was observed to move aft past the $\theta = 90$-deg location. The observation is consistent with transition to a turbulent boundary layer.

Blower Specifications and Description

The blower which provides the fairing suction was selected based on flow rate (m^3/min) and pressure differential (centimeters of water—cmH_2O). Initial calculations, utilizing the proposed fairing inlet area and a velocity equal to twice freestream velocity, yielded a flow rate of 200 m^3/min. Twice the freestream velocity was chosen from potential flow theory for flow about a cylinder. Potential flow theory also provided the required pressure differential. In order to eliminate the

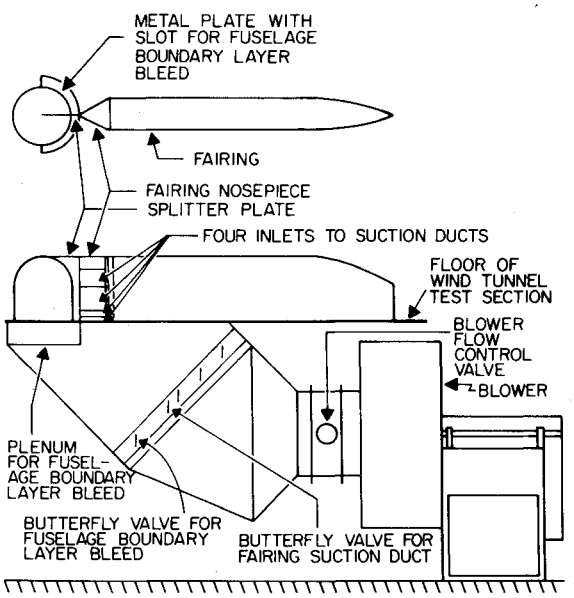

Fig. 1 Installation of turret, fairing nosepiece, fairing, fuselage boundary-layer bleed, suction ducting, and blower.

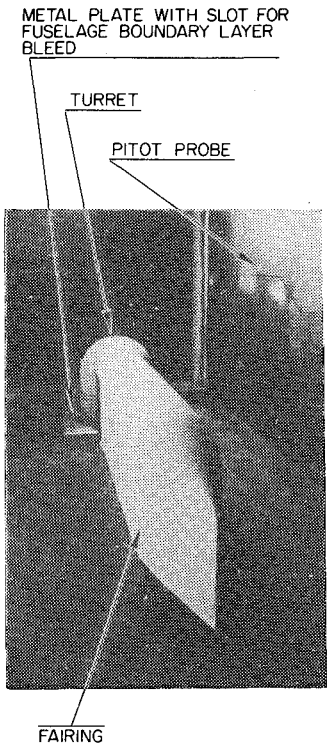

Fig. 2 View of turret and fairing assembly looking upstream.

adverse pressure gradient behind the turret model, a minimum pressure differential of three times the freestream dynamic pressure was desired. Using a freestream velocity of 10 m/s, freestream dynamic pressure is approximately 0.635 cmH_2O. To allow for losses within the ducting and to provide flexibility in possible follow-on experiments with higher velocities and pressure differentials, blower specifications were increased.

The blower has a capacity of 212 m^3/min with a static pressure differential of 35 cmH_2O. Figure 1 shows the blower installed below the floor of the wind-tunnel test section. A photograph of the blower and ducting is shown in Fig. 3.

Fairing Design

A hollow fairing with four internal ducts was constructed; each duct has a butterfly valve to throttle the flow. Figures 1 and 3 show the butterfly valve locations. Pitot-static tubes were installed in each duct. Consider a laser beam with a diameter which is one-half of the turret diameter. Using the geometry associated with the laser beam and turret, the fairing dimensions were such that a maximum turret look-back angle of 150 deg could be obtained.

Provisions were made for a detachable fairing nosepiece to allow variation of the turret/fairing geometry. Additionally, a plenum allowing for fuselage boundary-layer bleed at the base of the turret was incorporated into the fairing assembly. Figures 1 and 3 show the fuselage boundary-layer bleed. Both the turret and metal plate could be moved in the streamwise direction relative to the fairing and fairing nosepiece; hence the gap between the turret and fairing nosepiece could be varied. The turret and metal plate were connected together as a unit. Junctions were sealed with duct tape.

Fairing Nosepiece Designs

Two fairing nosepieces were designed and constructed. One fairing nosepiece was tested by Schonberger[7] and the other by Mandigo.[8] Figure 4 shows the fairing before the fairing nosepiece is installed; also, the turret and metal plate with slot for fuselage boundary-layer bleed are not installed. In Fig. 4, the four separate suction ducts are shown clearly; the plenum for fuselage boundary-layer bleed is shown also.

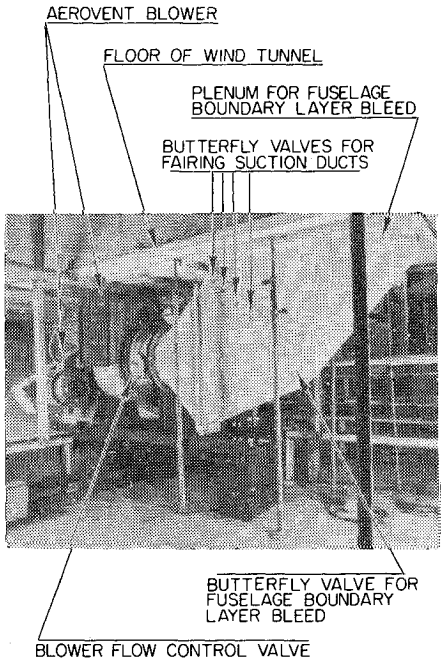

Fig. 3 Aerovent blower and ducting installed below the floor of the wind-tunnel test section.

The fairing nosepiece, which was tested by Mandigo,[8] was the uniform conformal nosepiece which is identified hereafter as UCN. The end nearest to the viewer is mated to the turret by a splitter plate. Figure 5 shows the UCN installed with the splitter plate against the turret surface. The gap between the UCN and the turret could be varied from 4.45 to 6.68 cm.

The fairing nosepiece, which was tested by Schonberger,[7] is shown in Fig. 6 and is identified as tapered symmetric nosepiece (TSN). Figure 1 was drawn with the TSN installed. The moveable metal plate permits adjustment of the inlet suction area. Once again, the distance between TSN and the turret could be varied; the range of variation was 1.27-11.43 cm. The TSN, as well as UCN, is connected to the fairing shown in Fig. 4.

Turret Design

A 0.3 scale model of the existing airborne optical system turret was constructed based on drawings provided by AFWL, USAF. The model consists of a hollow 0.427-m-diam circular cylinder, 0.244 m in height, topped by a 0.427-m-diam hemisphere. The turret is mounted on a 0.953-cm aluminum plate with a slot for fuselage boundary-layer

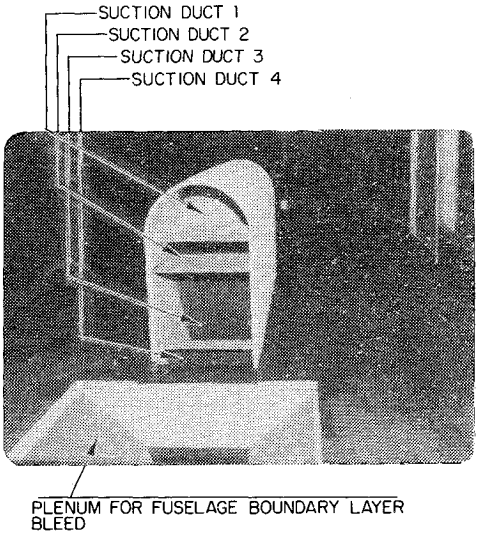

Fig. 4 Fairing without nosepiece installed; also plenum for fuselage boundary-layer bleed installed.

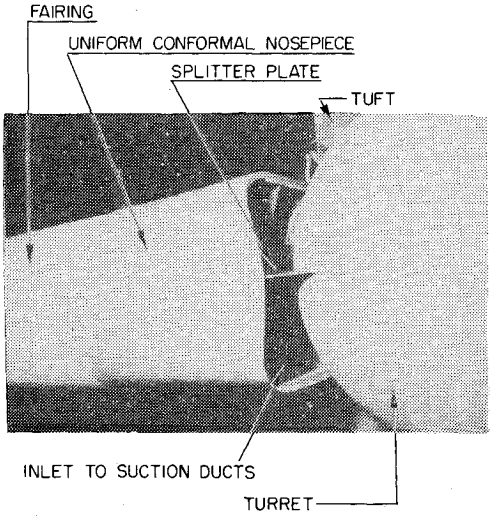

Fig. 5 Fairing nosepiece, fairing, splitter plate, and turret tested by Mandigo.[8]

suction. Figures 1, 2, and 5 show the turret. Figures 1 and 2 illustrate the metal plate with slot for fuselage boundary-layer bleed.

Instrumentation

Pressure Taps

Pressure taps were installed on the turret, in the wind tunnel, and in the duct assembly. Locations of the static pressure taps are given in the thesis by Schonberger.[7] As a result of the extensive array of pressure taps, the pressure distribution on the turret surface could be plotted. Knowledge of static pressure permits calculation of local velocity.

Wind-Tunnel Data Acquisition System

The wind-tunnel data acquisition system used in this research project consisted of an INTEL 80/10 Computer System, and AN/UGC-59A Teletypewriter Set, a 48-port Scanivalve, and a digital display unit for the Scanivalve. A control program for the Scanivalve was developed so that the pressure at each of the 48 ports could be measured. Each port of the Scanivalve is attached to its corresponding pressure tap via Tygon plastic tubing.

Tufts

In order to evaluate qualitatively the steadiness of the airflow, horizontal rows of tufts were taped to the turret. The tufts were made of a light yarn so that small airflow velocities caused displacement of the tufts. Definite tuft patterns were observed during separated flow condition; however, interpretation of the patterns was not attempted. The tufts clearly indicated the extent of the separated flow region.

Experiments and Experimental Results

Test Procedure

A test sequence was developed based on the requirement to investigate the following parameters: 1) turret position relative to the fairing; 2) fuselage boundary-layer suction; 3) fairing inlet area only with the tapered symmetric nosepiece (TSN); 4) total blower suction; and 5) control of fairing suction through the individual ducts. These tests were conducted for the two different fairing nosepieces. The test sequence included a step-by-step procedure to determine the combination of test variables which provide optimum flow stability. Optimum conditions were steady flow with the minimum amount of suction. These conditions were determined by tuft steadiness and turret pressure gradient measurements.

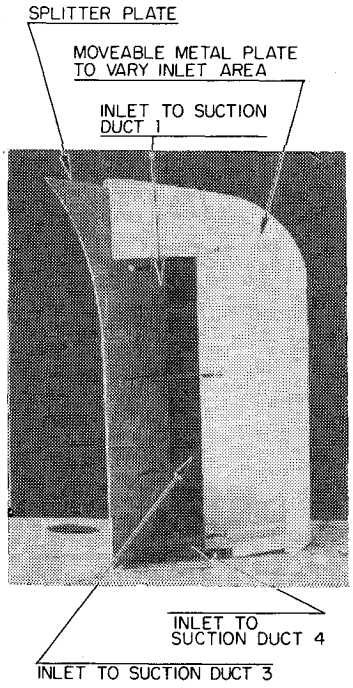

Fig. 6 Tapered symmetric nosepiece (TSN) tested by Schonberger.[7]

Data Recording

When the desired wind-tunnel conditions were attained, the data acquisition system was triggered manually. The pressure ratio, $\Delta P/q$, was calculated for each turret pressure tap and plotted vs port position. Reference static pressure, P_∞, was measured at the wind-tunnel wall near the turret position. Reference dynamic pressure, q, was measured with a pitot probe adjacent to the tunnel wall pressure port; see Fig. 2. Observations of tuft steadiness were recorded as well, and a color 16-mm movie of a test run with the tapered symmetric nosepiece, with and without flow control, was made.

Results with the Tapered Symmetric Nosepiece (TSN)[7]

The turret pressure distribution without flow control was measured as a baseline for comparison before the testing was started. For the baseline measurements, the apparatus was assembled completely as shown in Fig. 2.

The test series indicated that total blower suction of not less than 50% capacity is required for steady flow. The maximum fairing inlet area available is 0.093 m^2 with the adjustable cover plates in the open position. The tests, in this sequence, showed that a fairing inlet area of greater than 0.046 m^2 was required. The best flow in this series resulted when total blower suction of 50% and a fairing inlet area of 0.070 m^2 were employed.

The tests indicated no improvement in flow conditions when individual duct suction rates were varied. The optimum setting of the duct butterfly valves was therefore determined to be the fully open position.

The next series of tests resulted in a clear improvement in flow when fuselage boundary-layer suction was employed. Fuselage suction inlet area also was varied in this series. Optimum flow resulted with a fuselage suction inlet area of 0.011 m^2, a fairing inlet area of 0.070 m^2, a total flow suction of 113 m^3/min, and all butterfly valves fully open.

Another series of tests with the rear of the turret located 10 cm forward of the fairing indicated less stable flow. Figure 7a is a photograph of the turret with the wind tunnel on but without flow control suction; note the disarray of the tufts. Contrast this with Fig. 7b, which is a photograph of the turret with both the wind tunnel and the flow control activated; note the steadiness of the tufts with flow control employed. Figure 7 was obtained with UCN; similar results were obtained with TSN.

Data from one flow control experiment with TSN installed will be discussed now. The turret was located 1.27 cm from the TSN, and the splitter plate was touching the turret. The slot for fuselage boundary-layer bleed was fully open, and the butterfly valve for the fuselage boundary-layer bleed was fully open. The butterfly valves for the four suction ducts within the fairing were open completely. The blower valve was positioned to give a flow rate of 113 m^3/min. The fairing moveable metal plate shown in Fig. 6 was three-fourths open with an area of 0.070 m^2.

The turret pressure distribution is plotted in Fig. 8. Also plotted in Fig. 8 is the pressure distribution without flow control (curve 1) and the pressure distribution from potential flow theory (curve 2). The distributions for the test are those about the spherical portion (curve 3) and the cylindrical portion (curve 4) of the turret, while the other distributions are those about a cylindrical portion only. The cylindrical portion was used as a baseline for comparison since the separated flow was most difficult to control in this region. The word "cylinder" means data from pressure taps located on the cylindrical portion of the turret; the taps were in a plane located 9.4 cm above the tunnel floor. The word

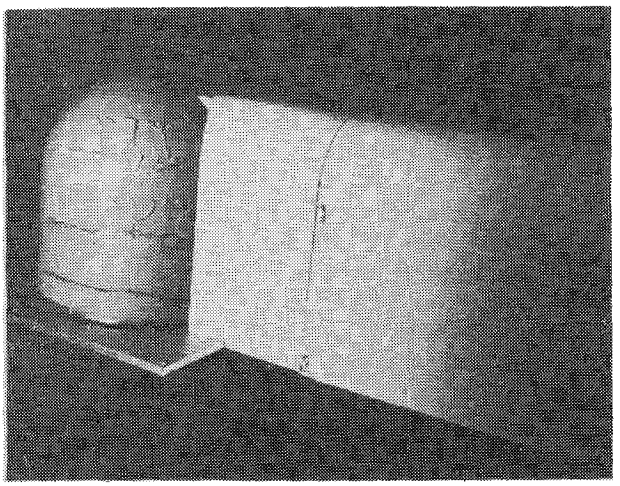

a)

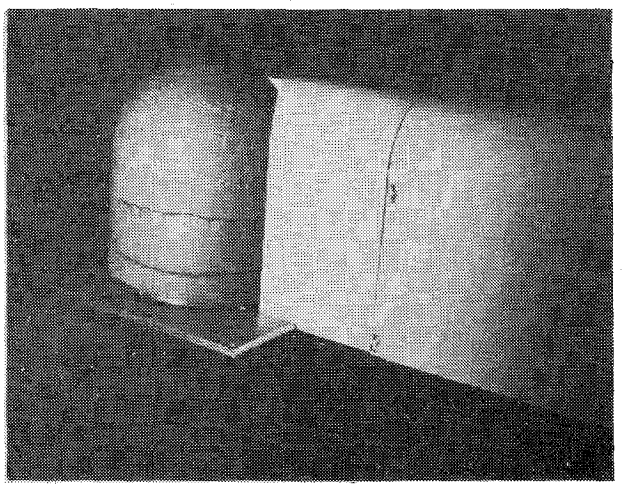

b)

Fig. 7 Demonstration effectiveness of flow control. In these photographs, the UCN is installed. a) Wind tunnel on; flow control off. b) Wind tunnel on; flow control on.

"sphere" means pressure taps located in the hemisphere of the turret; the taps are located in a fore-and-aft plane.

In Fig. 8, the adverse (increasing) pressure gradient from the 90-deg point to the 180-deg point can be seen (curve 1). However, with the flow control suction employed (curves 3 and 4), a favorable gradient exists at least to the 135-deg point. The dotted line from the 135-deg point to the 180-deg point (curve 4) is an attempt to extrapolate the pressure gradient between 135 and 180 deg. Without pressure taps in this region, the exact gradient is not known. However, based on tuft observations, the flow appears to remain steady to at least the 150-deg point, which implied that the favorable pressure gradient may extend beyond the 135-deg point.

Results with the Uniform Conformal Nosepiece (UCN)[8]

Results for several tests with the UCN now are described.

1. Turret-Fairing Nosepiece Separation Distance of 4.45 cm with Blower Damper Half-Open

Pressure coefficients that resulted from the test run with the blower damper half-open and all ducts open are plotted in Fig. 9. The theoretical pressure distribution plotted in Fig. 9 shows the expected adverse pressure gradient at the rear of the turret. The pressure distribution from the test run conducted at a separation of 4.45 cm shows a decrease in the pressure gradient at the rear of the turret. The decreased pressure gradient indicates that the suction does work.

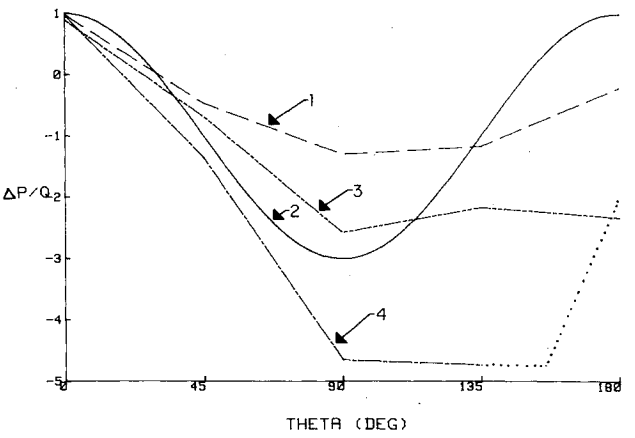

Fig. 8 Turret pressure distribution with and without flow control suction (TSN). 1) No flow control (cylinder); 2) theory (cylinder); 3) flow control on (sphere); 4) flow control on (cylinder).

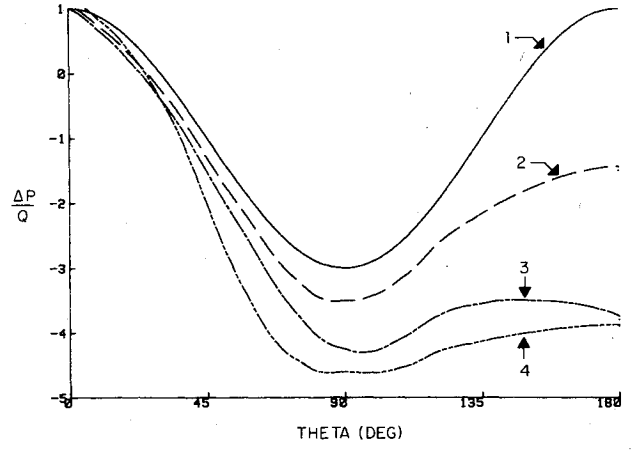

Fig. 9 Turret pressure distribution with and without flow control suction (UCN). 1) Potential flow theory for flow about an infinitely long cylinder. 2) Turret 4.45 cm, blower on; all ducts open, 50% flow. 3) Turret 4.45 cm, blower on; optimum flow condition, 18% flow. 4) Turret 6.67 cm, blower on; optimum flow condition, 28% flow.

2. Turret-Fairing Nosepiece Separation Distance of 4.45 cm with Variable Suction

Exploratory test runs were made using many flow configurations until the optimum configuration was found. Quiescent airflow around the turret was achieved when the tufts were steady and aligned with the local flow. Figure 7a is a photograph of the turret and fairing nosepiece with wind tunnel on but without blower suction. Note the disarray of the tufts. Figure 7b is a photograph of the turret and fairing nosepiece with suction; Fig. 7b was taken after the optimum flow configuration was achieved. Note that all of the tufts lie flat in the direction of flow, left to right. The optimum flow condition was achieved with the blower open to provide 18% of maximum flow, fuselage boundary-layer bleed open 25%, and the inlet ducts 1-4 open 100%, 100%, 50%, and 90%, respectively.

Pressure coefficients were evaluated for the 4.45-cm turret-fairing nosepiece separation distance and are plotted in Fig. 9. The 4.45-cm separation distance with optimum flow control configuration shows a flattened pressure distribution at the rear of the turret. The flattened pressure distribution means that boundary layer on the turret flows into a neutral pressure gradient.

The turret-fairing nosepiece separation distance of 4.45 cm provides steady airflow around the turret at a low blower suction volume flow rate (18% of blower maximum flow

capacity). The disadvantage of a small separation distance is the restriction on rearward look angle for the laser beam. The look angle for the 4.45-cm turret-fairing nosepiece separation distance is 125 deg; the beam diameter is assumed to be one-half of the turret diameter. This is a larger look angle than the current capability of 120 deg but is little geometrical improvement.

Comparing the test with all ducts fully open and the test with duct butterfly valves set optimally, one notes that both fuselage boundary-layer bleed slot and duct 3 were throttled significantly. Duct 3 is identified in Fig. 4. Decreasing the flow rate in duct 3 and the fuselage boundary-layer bleed slot allows greatly reduced blower suction.

3. Turret-Fairing Nosepiece Separation Distance of 6.67 cm with Variable Suction

Again exploratory test runs were made using many flow configurations until the optimum configuration was found, and quiescent airflow around the turret was achieved. The optimum flow condition was achieved with the blower open to provide 28% of maximum flow, fuselage boundary-layer bleed open 25%, and the inlet ducts 1-4 open 100%, 100%, 50%, and 90%, respectively.

Pressure coefficients were evaluated for the 6.67-cm turret-fairing nosepiece separation distance and are plotted in Fig. 9. The 6.67-cm separation distance with optimum flow control configuration shows a flattened pressure distribution at the rear of the turret. The flattened pressure distribution indicates that the increased turret-fairing separation distance also causes the boundary layer on the turret to flow into a neutral pressure gradient.

Scaling the Results to Full Scale

Scaling Results for the Tapered Symmetric Nosepiece[7]

The cross-sectional area of the upstream streamtube, A_∞, in the wind tunnel corresponding to flow rate of the blower, Q, was computed

$$A_\infty = Q/V_\infty = 1.88/9.97 = 0.190 \text{ m}^2$$

The value of Q was based on data provided by the blower manufacturer. Also each duct had a pitot-static probe which was used to determine duct velocity. With the inlet damper at 50% open $Q \simeq 113$ m^3/min $= 1.88$ m^3/s. A_∞ was compared with the presented area of the turret, A_t. The value of A_t for the model was 0.177 m^2. The flow factor F is defined as

$$F = A_\infty / A_t = 1.07 \tag{1}$$

The flow factor was used in scaling this test data to the actual aircraft configuration at a flight velocity $M_\infty = 0.5$.

The required flow rate, Q_r, was determined for incompressible flow to be

$$Q_r = Fa_\infty M_\infty A_t (60 \text{ s}/1 \text{ min}) \text{ m}^3/\text{min} \tag{2}$$

where A_t now represents the full-scale turret presented area. The value of A_t for the full-scale turret is 1.59 m^2.

The required pressure differential, ΔP_r, for the aircraft suction device was estimated based on turret pressure differential from the 135-deg point to ambient. An assumption of 70% pressure recovery in a fairing diffuser, π_r, was made, resulting in a pressure differential factor, n.

$$n = (1 - \pi_r)(\Delta P/q)_{135 \text{ deg}} = (0.3)(4.7) = 1.41$$

$$\Delta P_r = nq = n(\gamma/2) P_\infty M_\infty^2 \tag{3}$$

The values of Q_r and ΔP_r for various altitudes were computed using Eqs. (2) and (3) and are tabulated in Table 1. Pressure and sound velocity at altitude are from Ref. 9.

The tabulated results for Q_r were computed for incompressible flow. In order to estimate the minimum required fairing inlet suction area, A_s, and considering compressibility effects, choked flow was assumed at the inlet, i.e., $A_s = A^*$. Liepmann and Roshko[10] list the area ratio for choked flow at $M = 0.5$ as $A^*/A_\infty = 0.7464$. With $A_\infty = 1.07A_t = 1.70$ m^2, $A_s = 0.7464A_t = 1.27$ m^2. However, the fairing inlet area of the test model, if scaled up to full size, would be 0.727 m^2. The above computation indicates, therefore, that a larger fairing inlet area would be required for the actual aircraft configuration.

Scaling Results for the Uniform Conformal Nosepieces

Define a nondimensional separation distance, S, between the turret and fairing nosepiece

$$S = Z/D \tag{4}$$

where Z is the separation distance and D is the turret diameter. Scaling is discussed below for S equal to 0.104 and 0.156.

1. Nondimensional Separation Distance S Equal to 0.104

Volume flow rate and pressure difference across the blower were calculated using the above procedure and are tabulated in Table 2A. The results show that the volume flow rates and pressure differences are obtainable with present technology. One option is to install a J-85 turbojet in the fairing to provide suction.

The minimum fairing inlet suction area, A_s, would occur with choked flow; i.e., with $M_s = M^* = 1.0$. The value of the minimum allowable fairing inlet suction area is calculated by assuming $A_s = A^*$ and $A_\infty = FA_t$. With the area factor F, from experimental results, $A_\infty = FA_t = (0.398)(1.59) = 0.633$ m^2 and $A_s = 0.7464A_\infty = 0.472$ m^2 for the required suction area. However, the fairing inlet area of the test model, if scaled to full size, would equal 0.814 m^2. To summarize, model $A_s = 0.090$ m^2, full-scale $A_s = 0.814$ m^2, model $A_t = 0.177$ m^2, full-scale $A_t = 1.59$ m^2, full-scale $A^* = 0.472$ m^2, model $A_\infty = 0.054$ m^2 and full-scale $A_\infty = 0.633$ m^2. Therefore the previous computation indicates that the fairing inlet used in this experiment was 0.342 m^2 larger than required for the actual aircraft configuration. The inlet to the fairing should not choke.

2. Nondimensional Separation Distance S Equal to 0.156

Volume flow rate and pressure difference across the blower were calculated again, and the results are tabulated in Table 2B. The calculations show that the volume flow rates and pressure differences are greater than the values attained for

Table 1 Estimated Q_r and ΔP_r for full-scale application at various altitudes with tapered symmetric nosepiece

Altitude, ft	P, atm	a_∞, m/s	M_∞	ΔP_r, atm	Q_r, m^3/min
0	1	340.29	0.5	0.25	17,351
10,000	0.6878	328.39	0.5	0.17	16,747
20,000	0.4599	316.06	0.5	0.11	16,118
30,000	0.2978	303.23	0.5	0.07	15,464

Table 2 Estimated Q_r and ΔP_r for full-scale application at various altitudes with uniform conformal nosepiece

Altitude, ft	P, atm	a_∞, m/s	M_∞	ΔP_r, atm	Q_r, m^3/min
A. Separation distance = 4.45 cm, $F = 0.398$					
0	1	340.29	0.5	0.2066	6,455
10,000	0.6878	328.39	0.5	0.1421	6,232
20,000	0.4599	316.06	0.5	0.0950	5,995
30,000	0.2978	303.23	0.5	0.0615	5,752
B. Separation distance = 6.67 cm, $F = 0.619$					
0	1	340.29	0.5	0.2073	10,039
10,000	0.6878	328.39	0.5	0.1426	9,693
20,000	0.4599	316.06	0.5	0.0953	9,324
30,000	0.2978	303.23	0.5	0.0617	8,946

the 4.45 cm separation distance but are obtainable. For $Z = 4.45$ cm, S is 0.104.

Considering compressibility effects with choked flow at the inlet and using the area factor $F = 0.619$, the minimum required fairing inlet suction area A_s was 0.734 m^2. The test model, if scaled to full size, would be 0.814 m^2 as stated in the Flow Control Methods section. To summarize, model $A_s = 0.090$ m^2, full-scale $A_s = 0.814$ m^2, model $A_t = 0.177$ m^2, full-scale $A_t = 1.59$ m^2, full-scale $A^* = 0.734$ m^2, model $A_\infty = 0.110$ m^2, and full-scale $A_\infty = 0.983$ m^2. Therefore the computation indicates that even with the turret-fairing separation distance increased from 4.45 to 6.67 cm, the fairing inlet used is 0.080 m^2 larger than required for the actual aircraft configuration. Hence choked flow is avoided.

The 6.67-cm turret-fairing nosepiece separation distance ($S = 0.156$) increases the rearward look angle to 130 deg, which is an advantage. The disadvantage is the fact that blower suction was increased by 55%.

Conclusions and Recommendations

The concept of providing suction aft of a turret as a means of flow control has proven aerodynamically effective at critical Reynolds number in incompressible flow. The application of after-body suction in transonic flow at supercritical Reynolds number has not yet been demonstrated. If proven at transonic velocities, the requirements for flow control for the airborne laser could be met utilizing this concept. Other applications of after-body flow control, such as control about a forward-looking infrared (FLIR) turret, may be realized as well.

Total system implications of fairing suction have not been investigated as yet. Obviously, the method requires some means for providing suction in the fairing. The suction adds to overall system complexity and weight.

Testing at transonic velocities will be required to demonstrate the feasibility of flow control by after-body suction in airborne systems. Other turret/fairing geometries should be tested to achieve a maximum beam look-back angle while minimizing suction requirements. Laser beam quality with flow control employed also should be examined.

A silent 16-mm movie, 7 min in duration, is available on loan. The movie shows turret tuft motion with and without flow control employed. Requests should be directed to Professor Allen E. Fuhs.§

References

[1] Otten, L.J. III, "Overview of Recent Aero-Optics Flight Tests," *Proceedings of the Aero-Optics Symposium on Electromagnetic Wave Propagation from Aircraft,* NASA CP 2121, April 1980, pp. 363-395.

[2] Gilbert, K., "Lear Jet Boundary Layer/Shear Layer Laser Propagation Experiments," *Proceedings of the Aero-Optics Symposium on Electromagnetic Wave Propagation from Aircraft,* NASA CP 2121, April 1980, pp. 397-414.

[3] Walterick, R.E. and VanKuren, J.T., "Flow Visualization Techniques in the Airborne Laser Laboratory Program," *Proceedings of the Aero-Optics Symposium on Electromagnetic Wave Propagation from Aircraft,* NASA CP 2121, April 1980, pp. 537-565.

[4] McDermott, D.J. and VanKuren, J.T., "Validity of Small Scale Tests for Turret/Fairing Loads and Cavity Effects," *Proceedings of the Aero-Optics Symposium on Electromagnetic Wave Propagation from Aircraft,* NASA CP 2121, April 1980, pp. 615-656.

[5] Schlichting, H., *Boundary Layer Theory,* 6th ed., McGraw-Hill Book Co., New York, 1968.

[6] deJonckheere, R., *Control of Turbulent, Separated Airflow about Aircraft Turrets,* Workshop Notes from the Air Force Weapons Laboratory Workshop, Albuquerque, N. Mex., March 1980.

[7] Schonberger, J., "Flow Control about an Airborne Laser Turret," M.S. Thesis, Naval Postgraduate School, Monterey, Calif.; see also NPS 67-80-018.

[8] Mandigo, A., "Control of Airflow about a High Energy Laser Turret," M.S. Thesis, Naval Postgraduate School, Monterey, Calif.; see also NPS 67-80-019.

[9] *U.S. Standard Atmosphere, 1976,* National Oceanic and Atmospheric Administration, National Aeronautics and Space Administration, USAF, U.S. Government Printing Office, 1976.

[10] Liepmann, H.W. and Roshko, A., *Elements of Gas Dynamics,* Wiley and Sons, New York, 1957.

§Address: Code 67Fu, Department of Aeronautics, Naval Postgraduate School, Monterey, Calif. 93940; telephone: commercial, 408-646-2948, or AUTOVON, 878-2948.